

Glucose in dry and moist ionic liquid: Vibrational circular dichroism, IR, and possible mechanisms

Supporting information

Jan Blasius^a, Roman Elfgen^a, Oldamur Hollóczy^a, and Barbara Kirchner^{a,*}

^aMulliken Center for Theoretical Chemistry, Institute for Physical and
Theoretical Chemistry, University of Bonn, Berlingstr. 4+6, D-53115 Bonn,
Germany

*kirchner@thch.uni-bonn.de

February 27, 2020

Keywords:

Glucose, Ionic Liquids, Ab Initio Molecular Dynamics Simulations, Infrared Spectroscopy,
Vibrational Circular Dichroism Spectroscopy

1 Computational Details

1.1 Systems investigated

Three different types of glucose molecules, the open chain glucose, and the closed ring α - and β -glucose (cf. Figure S1), were chosen as model systems to investigate the solvent effect of the ionic liquid 1-ethyl-3-methylimidazolium acetate ($[\text{C}_2\text{C}_1\text{Im}][\text{OAc}]$), with and without water, on the glucose IR and VCD spectra. In case of the water-free systems, 8 glucose molecules were surrounded by 48 IL ion pairs of the IL, whereas in the water-containing systems 6 glucose molecules were surrounded by 36 ion pairs and additionally 100 water molecules, see also table S1.

Table S1: Compositions of the simulation boxes.

quantity	O/A/B	OW/AW/BW
No(IP)	48	36
No(glu)	8	6
No(wat)	—	100
wt%(wat)	—	20
c(glu) / g(glu)/mol(IL)	30.0267	30.0267
wt%(glu)	15	11
t _{sim} / ps	43/38/40	47/39/49

1.2 Setting up the simulation box through classical molecular dynamics simulations

With the aid of the program PACKMOL,^{1,2} the components of each system **A** and **AW** were first placed into a cubic simulation box to represent a density of 1 gm cm³. The simulation boxes were then simulated with the LAMMPS program,³ in an NpT ensemble at a temperature of 350 K and under 1 bar pressure for 1 ns, using the force field parameters of

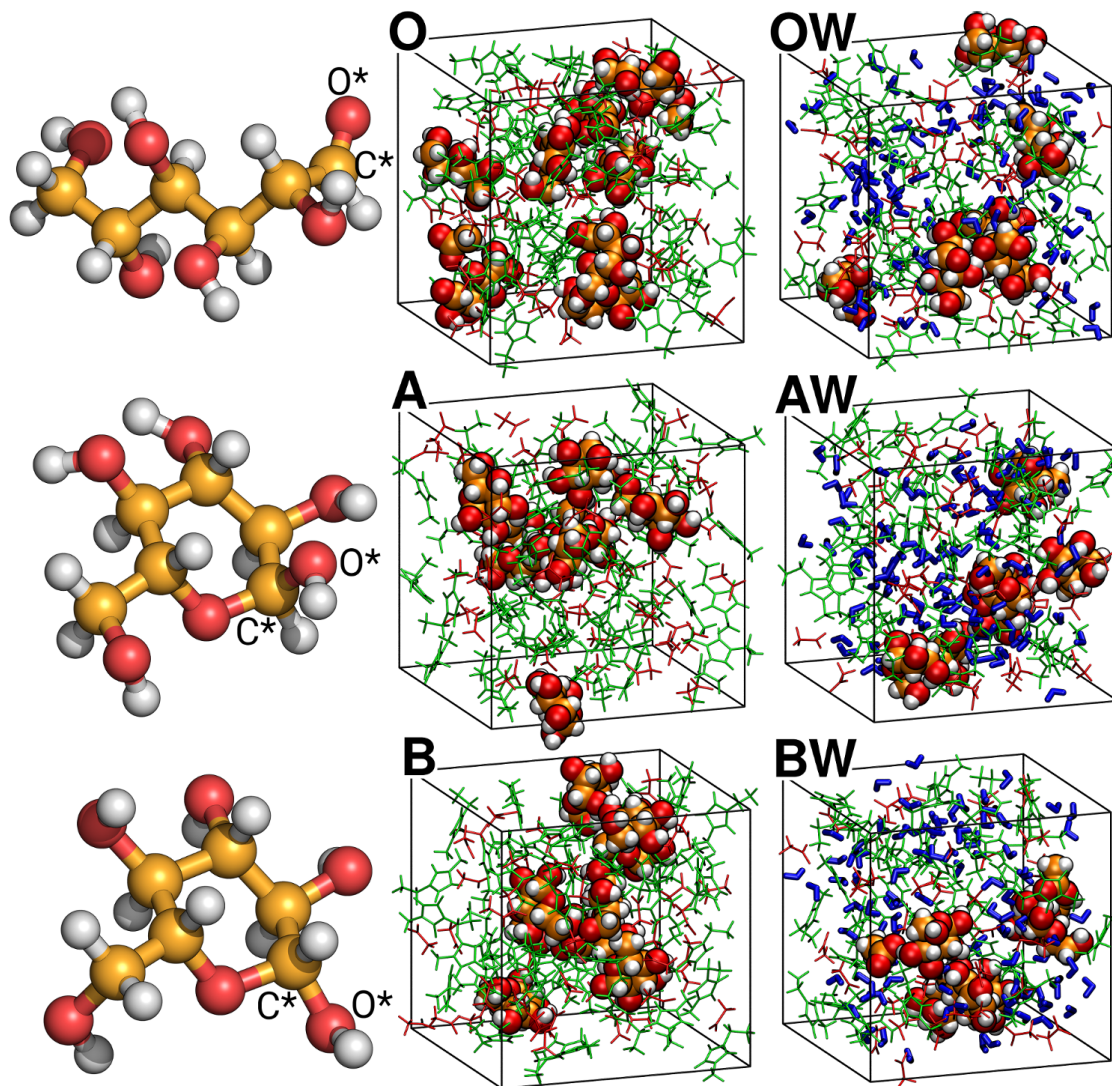


Figure S1: Ball-and-stick images of different glucose molecules and snapshots of simulation boxes without water (O, A and B) and with water (OW, AW and BW). The upper row shows the open chain glucose, the middle row α -glucose and the bottom row β -glucose. Within the simulation boxes the IL cations are colored in green, the IL anions in red and the water molecules in blue.

Padua and Canongia Lopes for the ionic liquid,^{4,5,6} and the SPC/E model for water.⁷ Over the last 0.5 ns of these simulations, the volume of each box was averaged. The resulting cell vectors were 2423.88 pm for the dry systems and 2372.30 pm for the moist systems (cf. Figure S1), which are expected to be similar to experimental values.

1.3 AIMD Simulations

The resulting geometries were then used for the subsequent AIMD simulations, which consisted of three steps: Geometry optimization, equilibration run and production run. All three steps were carried out using density functional theory (DFT) within the CP2K⁸ program package applying the QUICKSTEP module.⁹ Here, the hybrid Gaussian and plane waves (GPW) approach was used to calculate the energies and forces on the atoms. The molecularly optimized double- ζ basis set (MOLOPT-DZVP-SR-GTH)¹⁰ was applied to all atoms together with the BLYP functional and the corresponding BLYP Goedecker–Teter–Hutter pseudopotentials for core electrons.^{11,12,13} A 280 Ry density CUTOFF criterion with the finest grid level was employed, together with multigrids number 5 (NGRID 5 and REL_CUTOFF 40 (30 for the geometry optimization)) using the smoothing for the electron density (NN10_SMOOTH) and its derivative (NN10).⁹ Dispersion interactions were accounted for by applying the DFT-D3 type of a pair potential van der Waals density functional.^{14,15} For the SCF calculation, the default value (10^{-5}) was used as target accuracy for the SCF convergence. The DIIS minimizer⁸ was used to reach a faster orbital transformation via direct inversion in the iterative subspace. The maximum number of SCF iterations to be performed for one iteration was set to 200 (geometry optimization: 20 iterations for inner, 10 iteration for outer SCF).

The geometry optimization was performed applying the conjugate gradient minimization method using a value of 10^{-3} as a convergence criterion for the maximum geometry change between the current and the last optimizer iteration as well as for the maximum force component of the current configuration (MAX_DR, MAX_FORCE). The same value was used as a convergence criterion for the root mean square (RMS) geometry change and force (RMS_DR,

RMS_FORCE). The maximum number of iterations was set to 100.

In order to observe and analyze the temporal development of the systems over time, the following equilibration and production runs were carried out applying periodic boundary conditions in order to avoid boundary effects. The canonical (NVT) ensemble was used with the aid of the Nosé–Hoover-chain thermostats^{16,17} with a time constant of the thermostat chain of 100. The equilibrations were performed over 7.5 ps (15000 steps à 0.5 fs) defining the keyword REGION MASSIVE and raising the temperature to 500 K to achieve faster equilibration. The subsequent production runs were carried out at the temperature of 350 K.

For the following analyses the first 15000 time steps of the trajectories were neglected to avoid effects from the previous equilibration with massive thermostats.

1.4 Analysis

Our open source program TRAVIS (Trajectory Analyzer and Visualizer) was used to examine the time-dependent structural development of the simulated systems and to calculate IR and VCD spectra of the differently situated glucose molecules.¹⁸ The results are visualized with the aid of the xmgrace software¹⁹ or, alternatively, the program gnuplot (version 5.0)²⁰ for the generation of three-dimensional plots of data.

Structural Characterization

The dissection of the systems into domains can be realized by defining their individual building blocks, i.e. subsets.²¹ These subsets can be functional groups, parts of the molecules, complete molecular entities or even groups of molecules. For the systems investigated here, we distinguish six subsets based on the following units: Cation and anion (IL), cation (Cat), anion (An), glucose (Glu), glucose and anion (Glu+An) and water (W). A radical Voronoi tessellation is performed, in which all atoms are considered as Voronoi sites s_i to uniquely divide the Euclidean space into a set of Voronoi cells, assigning each point in space to exactly one cell. In that way, each cell consists of all points that are closer to a particular site than

to any other. To correctly model the intra- and intermolecular distances when constructing the Voronoi cells, additionally van der Waals radii r_i are assigned to each site, and the distance to the sites is replaced by the power distance to circles around the sites with the corresponding radii:

$$C_i = \{x \in \mathbb{R}^3 \mid (x - s_i)^2 - r_i^2 \leq (x - s_j)^2 - r_j^2 \forall j \neq i\}; \quad i, j = 1, \dots, n. \quad (1)$$

Therein, n describes the number of sites s_i . The resulting atomic Voronoi cells C_i are then summed up according to the subsets defined before. The subsets belong to the same domain if their cells share a common face. This allows for determining the average number of each kind of domain present in the liquid, which we call the domain count N_{Dom} . Any value for N_{Dom} smaller than the total number of the particular subsets that constitute it represents a certain level of aggregation in the system. If the domain count is one, it means that the subsets are forming a large, continuous network that stretches through the system.

Next to the possibility to perform a domain analysis, TRAVIS also enables the time-dependent investigation of structural features of the solvent and the solute, intra- and intermolecular interactions within or between the components and the elucidation of chemical reaction mechanisms by calculating different distribution functions (DFs) between relevant atoms or centers of the observed molecules. The most used features are radial, angular, distance and spatial distribution functions (RDFs, ADFs, DDFs and SDFs, respectively) but also combined distributions functions, which are three-dimensional plots that combine two DFs with each other.

Calculation of Vibrational Spectra

The calculation of different spectroscopic properties in liquid media and for flexible molecules was introduced by Green and Kubo,^{22,23} who showed that phenomenological coefficients describing many transport processes and time-dependent phenomena can be written as integrals over auto-correlation functions. In order to decompose the auto-correlation functions into their particular constituent frequencies, a Fourier transformation using the Wiener-

Khintchine theorem is applied:^{24, 25}

$$\langle C(\tau)C(t + \tau) \rangle_\tau = \frac{1}{2\pi} \int \left| \int f(t)e^{-i\omega t} dt \right|^2 e^{i\omega t} d\omega. \quad (2)$$

The intensity of the resulting spectrum corresponds to the amplitude of the oscillation in the correlation function and thus, notable changes in the molecular properties that are active for a given type of spectroscopy (i.e. the molecular dipole moments in case of IR spectroscopy) lead to peaks in the spectrum and vice versa. In the next step the harmonic approximation for the intensities is applied. Since the amplitude of a distinct normal mode in mass-weighted coordinates is inversely proportional to the eigenfrequency ω , the oscillations of the molecular dipole moment are multiplied by $1/\omega$. Due to the fact that the products of these quantities enter the correlation functions, after the Fourier transformation the whole spectrum needs to be multiplied by ω^2 . Using the time derivative, which is advantageous due to numerical reasons, the IR intensities $A(\omega)$ are then given by

$$A(\omega) = \frac{N_A}{24\pi\epsilon_0 c^2 k_B T} \int \langle \dot{\mu}(\tau) \cdot \dot{\mu}(t + \tau) \rangle_\tau e^{-i\omega t} dt. \quad (3)$$

For comparison to experimental data, the corresponding wavenumber-dependent representation is

$$A(\tilde{\nu}) = \frac{N_A}{12\epsilon_0 c k_B T} \int \langle \dot{\mu}(\tau) \cdot \dot{\mu}(t + \tau) \rangle_\tau e^{-2\pi i c \tilde{\nu} t} dt. \quad (4)$$

With the Avogadro constant N_A (in mol⁻¹), the electric constant ϵ_0 (in C² s² kg⁻¹ m⁻¹), the speed of light c (in m s⁻¹) the Boltzman constant k_B (in m² kg s⁻² K⁻¹), the temperature T (in K), the electric dipole moment μ (in C m), the time t/τ (in s) and the wavenumber $\tilde{\nu}$ (in m⁻¹) the IR intensity possesses the unit m² mol⁻¹. For more details see Ref.²⁶

While the fundamental quantity associated with the IR absorption is the dipole strength, the differential absorption is also proportional to the rotational strength, a quantity which depends on both the electric and magnetic dipole transition moments μ and M , respectively. According to this, Abbate et al.²⁷ developed the time-correlation ansatz for the calculation of VCD spectra from molecular dynamics trajectories, which is based on a cross-correlation of the electric and magnetic dipole moment:

$$A(\omega) = \frac{N_A}{24\pi\epsilon_0 c^3 k_B T} \int \langle \dot{\mu}(\tau) \cdot \dot{M}(t + \tau) \rangle_\tau - \langle \dot{M}(\tau) \cdot \dot{\mu}(t + \tau) \rangle_\tau e^{-i\omega t} dt, \quad (5)$$

The corresponding wavenumber-dependent expression is

$$A(\omega) = \frac{N_A}{12\varepsilon_0 c^2 k_B T} \int \langle \dot{\mu}(\tau) \cdot \dot{M}(t + \tau) \rangle_\tau - \langle \dot{M}(\tau) \cdot \dot{\mu}(t + \tau) \rangle_\tau e^{-2\pi i c \bar{\nu} t} dt. \quad (6)$$

Please note that compared to the IR intensity, the VCD intensity possesses a slightly modified prefactor regarding the speed of light c . Nevertheless, the VCD intensity possesses the unit $\text{m}^2 \text{mol}^{-1}$, as well. The magnetic dipole moment is calculated via the electric current density, for more details see Ref.²⁸

For the calculation of the electric dipole moments the radical Voronoi tessellation is applied as well (cf. equation (1)). Here, however, all Voronoi cells C_i of all atoms belonging to the same molecule are united in order to receive molecular cells M_k . The recognition of the molecules is available in TRAVIS.¹⁸ Molecular dipole moments can now be obtained by integrating the electron density $\rho(r)$, which is accessible for each time step in an AIMD simulation, as a function of the spacial coordinate r over the afore defined molecular cells:

$$\mu = \int_{M_k} r \cdot \rho(r) dr; \quad k = 1, \dots, N. \quad (7)$$

1.5 Computation of the Gibbs free energy in solution

In order to calculate the Gibbs free energies for the isomerization of the different glucose isomers in solution, the following workflow has been applied. The Gibbs free energy of the reactions ΔG_{soln} can be written as

$$\Delta G_{soln} = \Delta E_{gas} + \Delta G_{therm} + \Delta G_{solv}, \quad (8)$$

with ΔE_{gas} being the quantum chemical gas phase energy difference, ΔG_{therm} is the thermodynamic Gibbs free energy difference and ΔG_{solv} describes the free energy of solvation difference between product and reactant. To calculate the different contributions, it is crucial to have geometries of the involved molecules which represent minimum structures in the best case. We obtained a variety of 200 different monomeric structures for each glucose isomer by cutting 100 structures from the AIMD simulations for the dry and wet systems, respectively. The cutting procedure was carried out using TRAVIS. Since optimizations on

accurate levels of theory can become very costly, especially for such a huge amount of individual geometries, the geometry optimizations were carried out using the low-cost PBEh-3c²⁹ method with subsequent single-point calculations on the obtained structures at PW6B95³⁰-D3^{14,15}/def2-QZVP³¹ level of theory. Thermodynamics were calculated at the semiempirical GFN2-xTB³² level by re-optimizing the PBEh-3c geometries and subsequent calculation of the vibrational frequencies. The solvation free energies were computed with the COSMO-RS solvation model.^{33,34} Generally it not necessary to use the same computational method for the COSMO-RS calculation and the calculation of the electronic energy and thermodynamic Gibbs free energy. In this study we used the BP-TZVPD-FINE level of theory, which is considered to yield the "best quality" and uses a single-point COSMO surface charge calculation on BP DFT with def2-TZVPD basis set. The BP-TZVPD-FINE level is implemented in the Turbomole^{35,36} software package which we used for our purposes. For each of our investigated systems (open chain, α - and β -glucose in a dry and wet system, respectively) we chose the geometry and its corresponding energy contributions for the structure with the lowest Gibbs free energy of solvation. Finally, knowing all the individual energy contributions the reaction Gibbs free energies for the isomerization between the glucose isomers have been calculated according to equation 1.5.

2 Results and Discussion

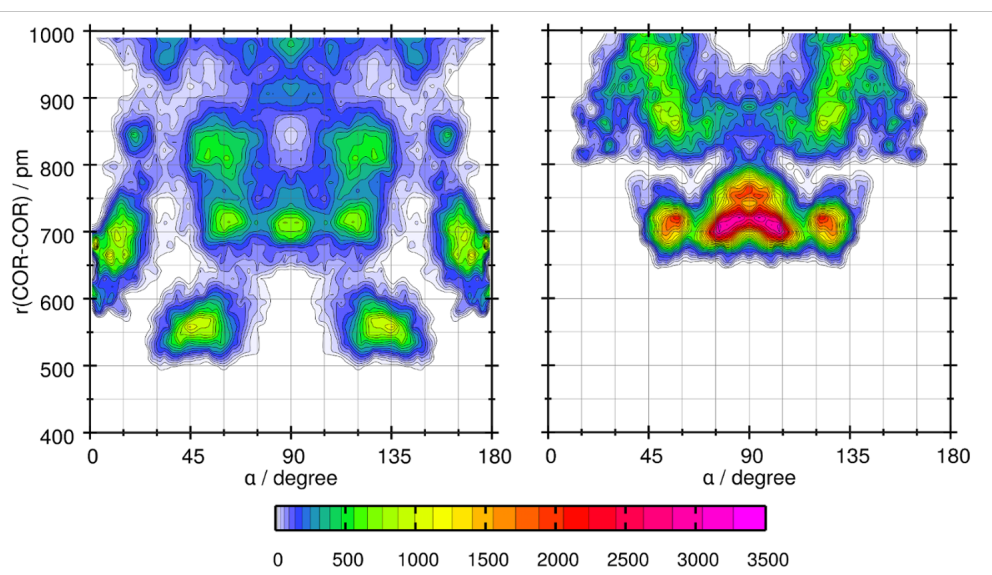


Figure S2: Shown is a combined distribution function for the **A** (left) and the **AW** (right) systems to analyze the stacking of the rings. α indicates the angle between the ring normal of the reference molecule and the vector which is defined by the center of ring center of ring (CoR)-CoR-distance of the α -D-glucose observed molecule. While 0 and 180 degrees indicate a stacked system, 90 degrees indicates an in-plane arrangement. More detailed information about this can be found in Refs.^{37,38}

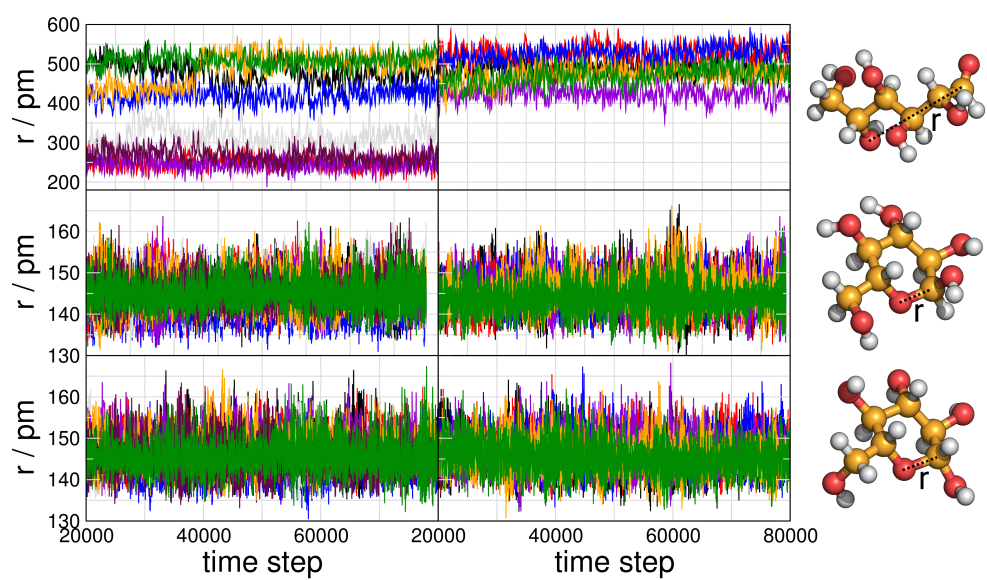


Figure S3: Temporal development of the distance r (see right) for all simulated glucose molecules. The upper panels refer to **O** (left) and **OW** (right), the middle panels are due to **A** (left) and **AW** (right) and the lower panels belong to **B** and **BW**. Colors represent different glucose molecules.

2.1 Overall structure

2.2 Hydrogen bond structure

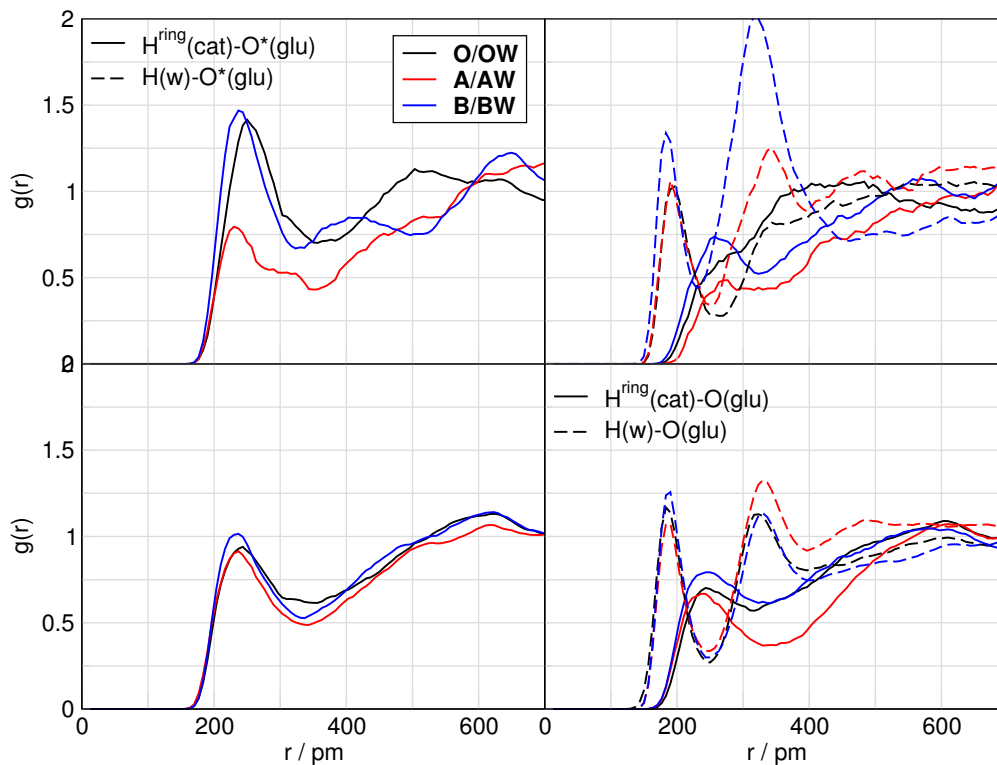


Figure S4: Radial distribution functions (RDFs) between the ring protons H^{ring} of the cation and the oxygen atom O^* bound to the specifically labeled stereo center (see Figure S1) of glucose (upper plots) and all glucose oxygen atoms (bottom plots). Dotted lines are the same for the water protons $H(w)$.

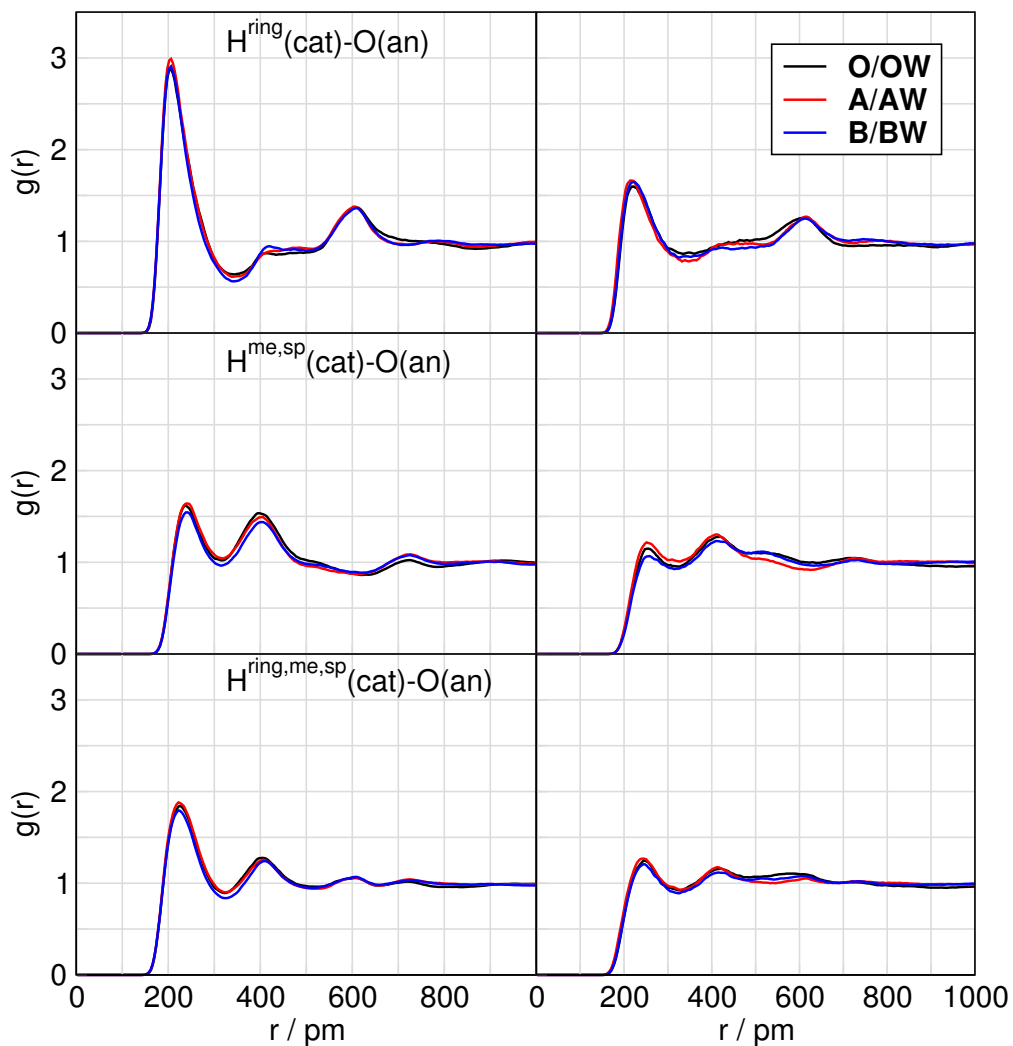


Figure S5: Radial distribution functions (RDFs) between the acidic protons of the cation and the oxygen atoms of the anions. H^{ring} includes only the ring hydrogens, $H^{\text{me,sp}}$ the hydrogen atoms of the methyl group and the CH_2 spacer of the ethyl group and $H^{\text{ring,me,sp}}$ includes all hydrogen atoms of the ring, the methyl group and the ethyl spacer.

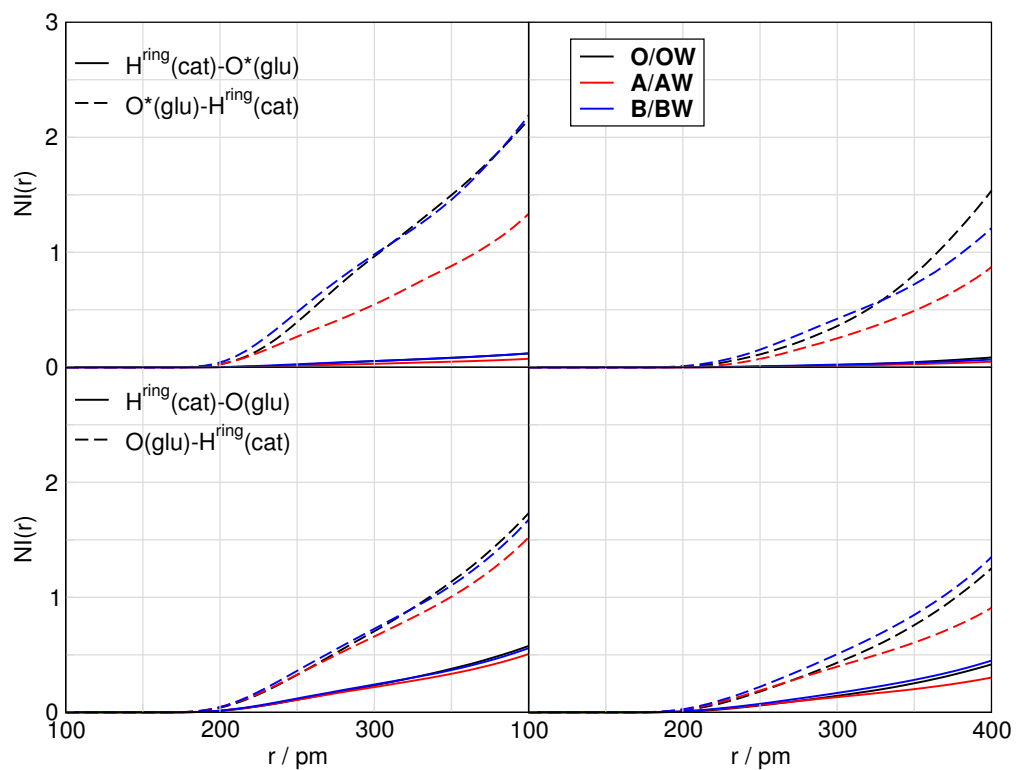


Figure S6: Number integrals $NI(r)$ between the ring protons H^{ring} of the cation and the oxygen atom O^* bound to the specifically labeled stereo center (see Figure S1) of glucose (upper plots) and all glucose oxygen atoms (bottom plots). The left column shows the systems without water, the right column the systems with water.

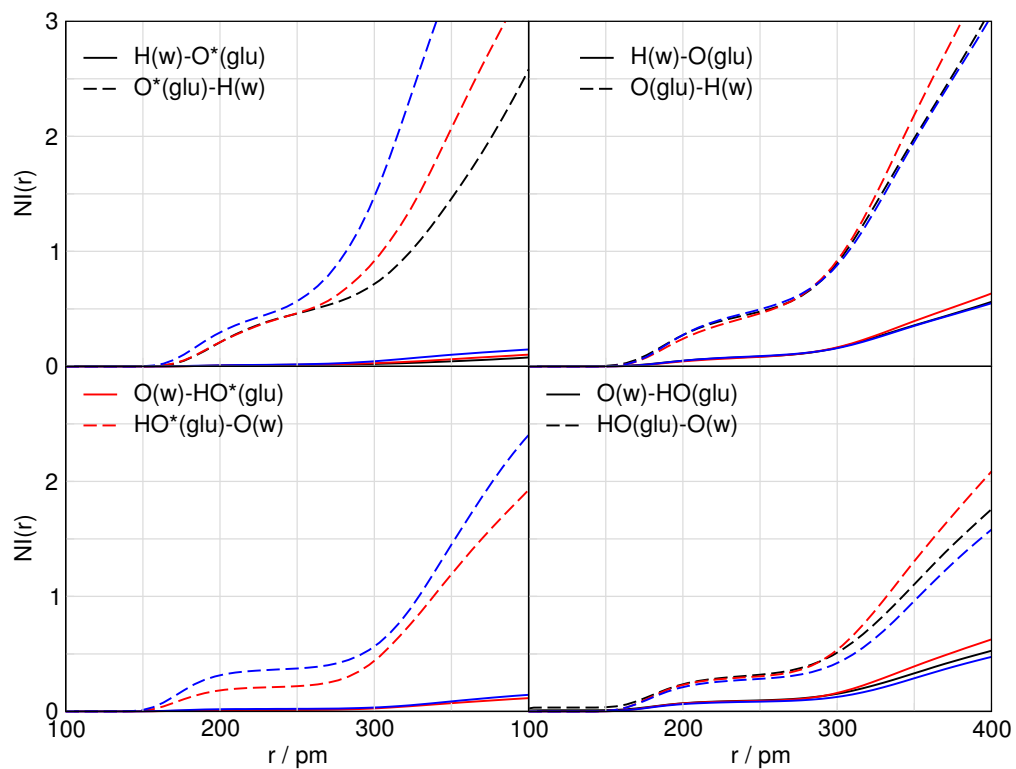


Figure S7: Number integrals $NI(r)$ between water and glucose. The upper row shows the $H(w)-O(glu)$ and the lower row the $O(w)-H(glu)$ interplay. The left column depicts the interactions of water with the oxygen atom O^* bound to the specifically labeled stereo center (see Figure S1) of glucose, the right column shows the interaction of water with all oxygen atoms of glucose.

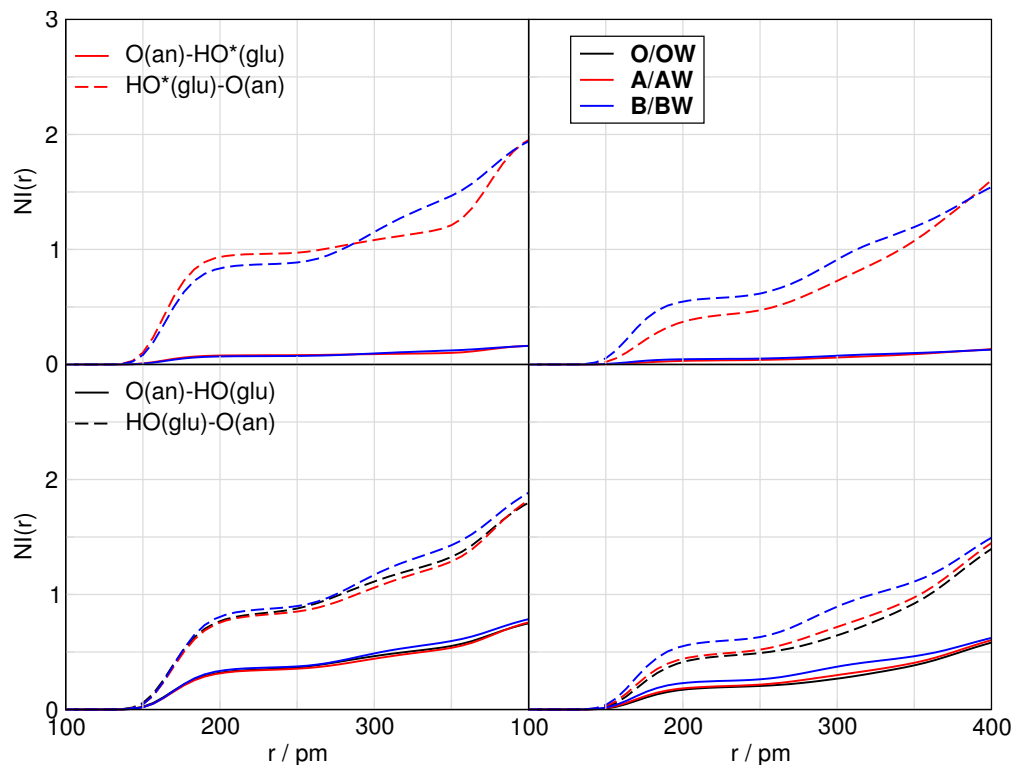


Figure S8: Number integrals $NI(r)$ between the anion oxygen atoms and the glucose hydrogen atom associated with the specifically labeled stereo center (see Figure S1) of the molecule (upper plots) and all alcohol-hydrogen atoms at the glucose molecules (bottom plots). Please note, the open form stereo center oxygen atom is transformed into an aldehyd group which is why the curves for the open form are missing above. The left column shows the water free systems, the right column the systems including water.

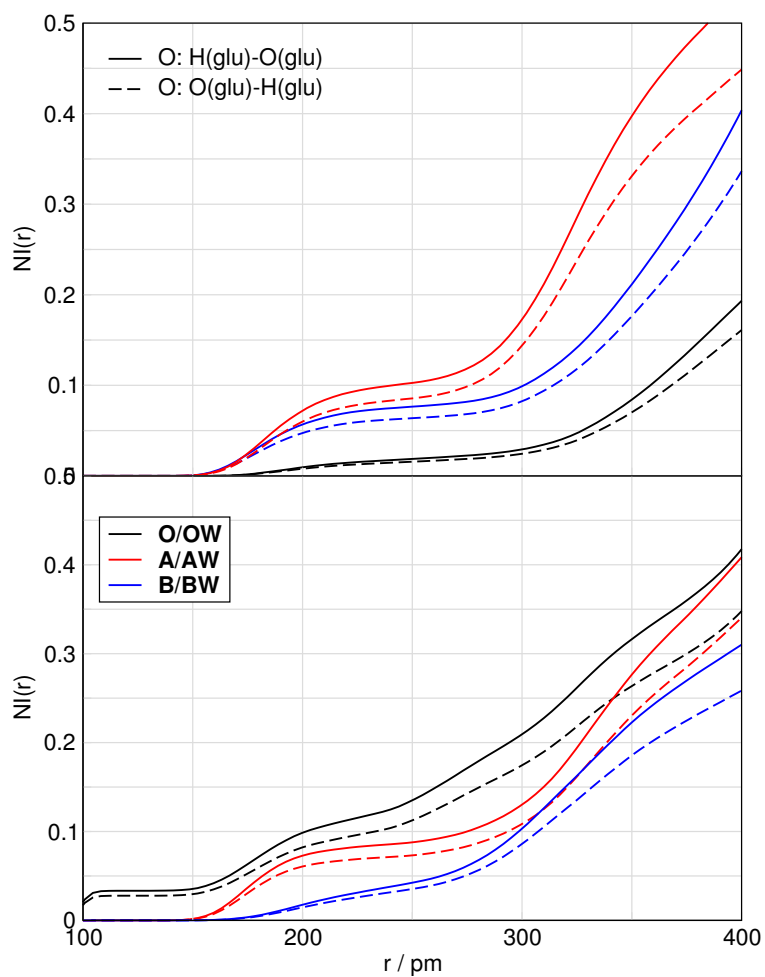


Figure S9: Number integrals NIs of the intermolecular distances between all alcohol-hydrogens and all oxygen atoms of glucose. The upper plot shows the water free systems, the lower plot the systems containing water.

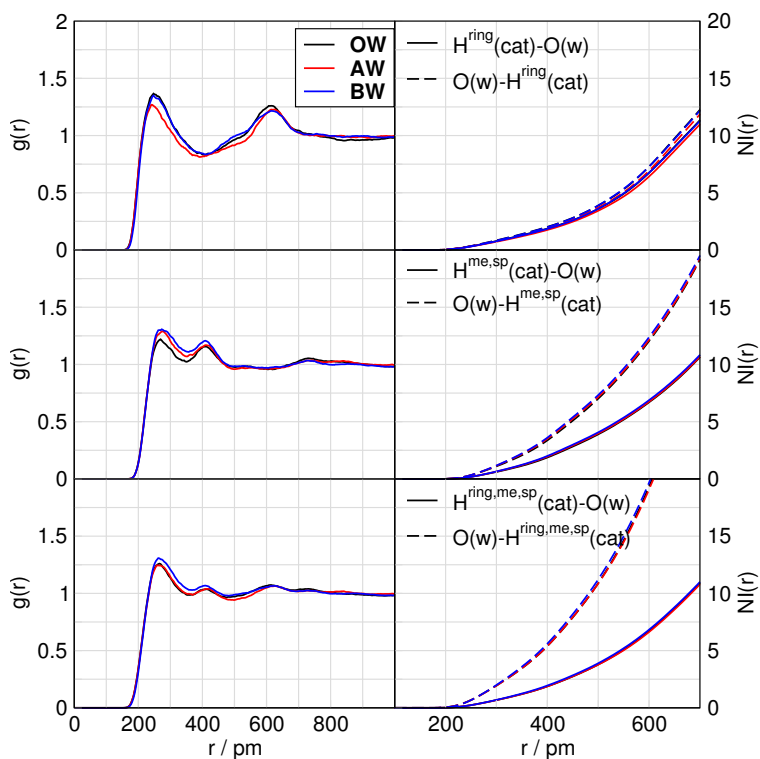


Figure S10: Radial distribution functions (RDFs) and number integrals NIs between the acidic hydrogen atoms of the cation and the oxygen atoms of water. H^{ring} includes only the ring hydrogens, $H^{\text{me,sp}}$ the hydrogen atoms of the methyl group and the CH_2 spacer of the ethyl group and $H^{\text{ring,me,sp}}$ includes all hydrogen atoms of the ring, the methyl group and the ethyl spacer.

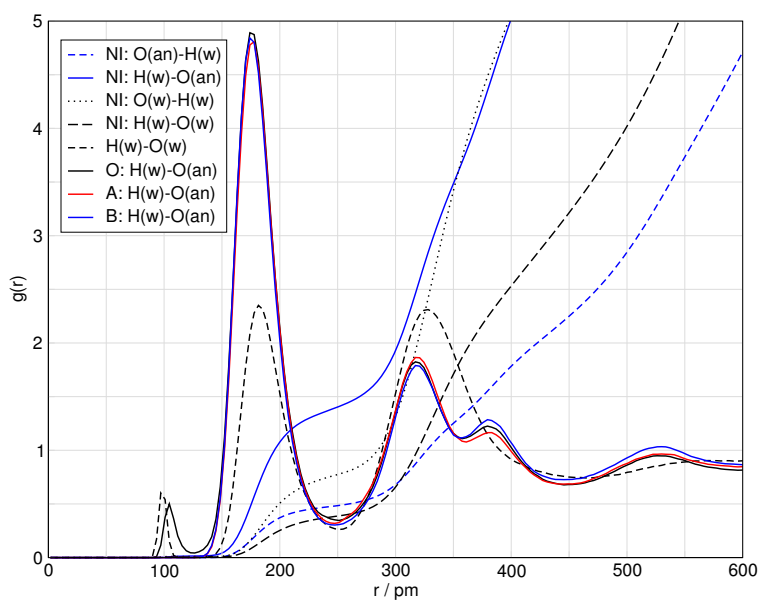


Figure S11: Radial distribution functions (RDFs) and number integrals NIs between the oxygen atoms of the anions and the hydrogen atoms of water as well as between both, the hydrogen atoms and oxygen atoms of water.

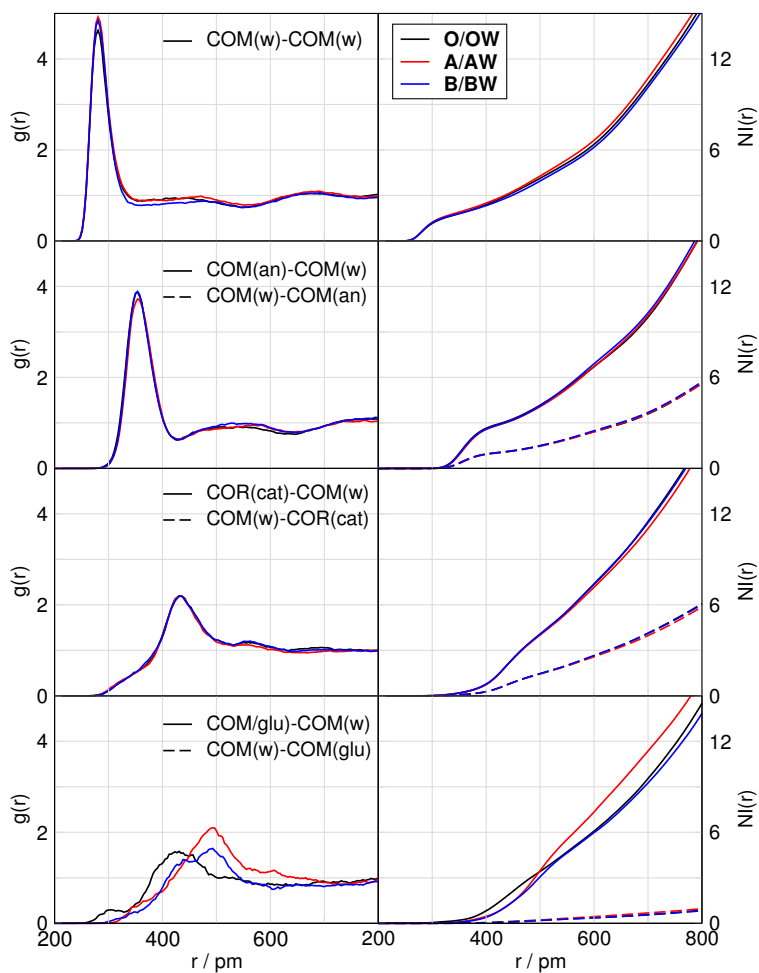


Figure S12: Radial distribution functions (RDFs) and number integrals NIs between the center of mass of water and the center of masses of glucose and anion as well as the center of ring of the cation.

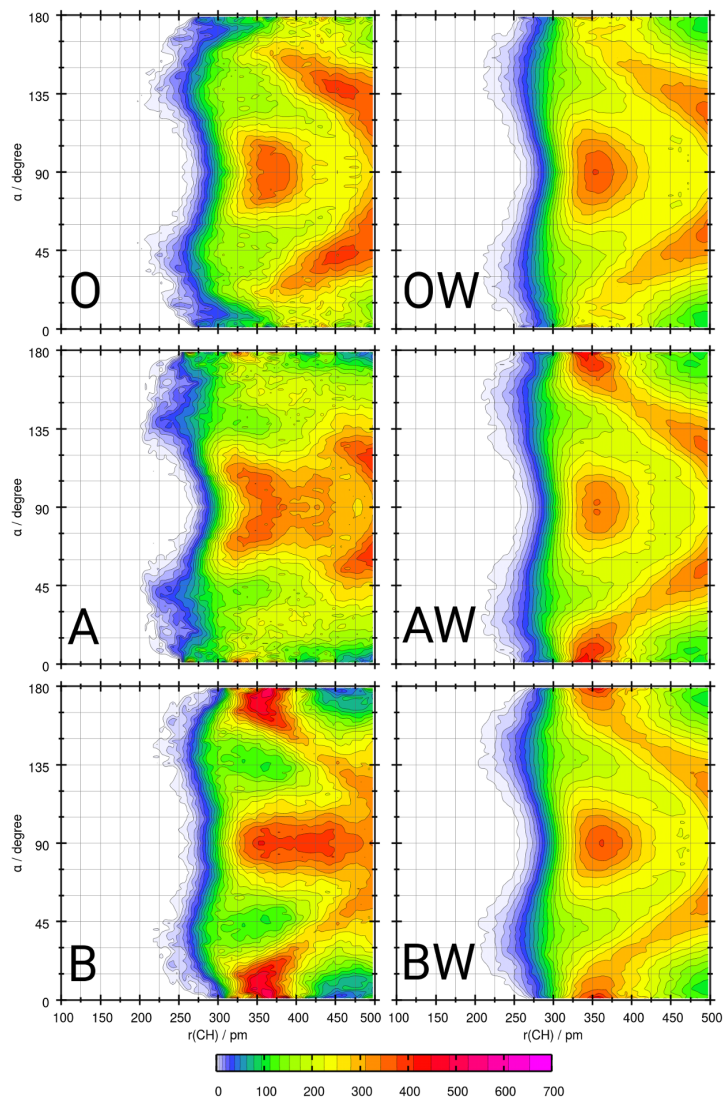


Figure S13: Combined distribution functions (CDFs) showing the distance of the ring carbons of the cations to all acidic hydrogen atoms donated by an oxygen atom on the x-axis and the angle of vector build by the acidic hydrogen atom and the center of ring of the cation to the ring normal of the cation.

2.3 Spectra

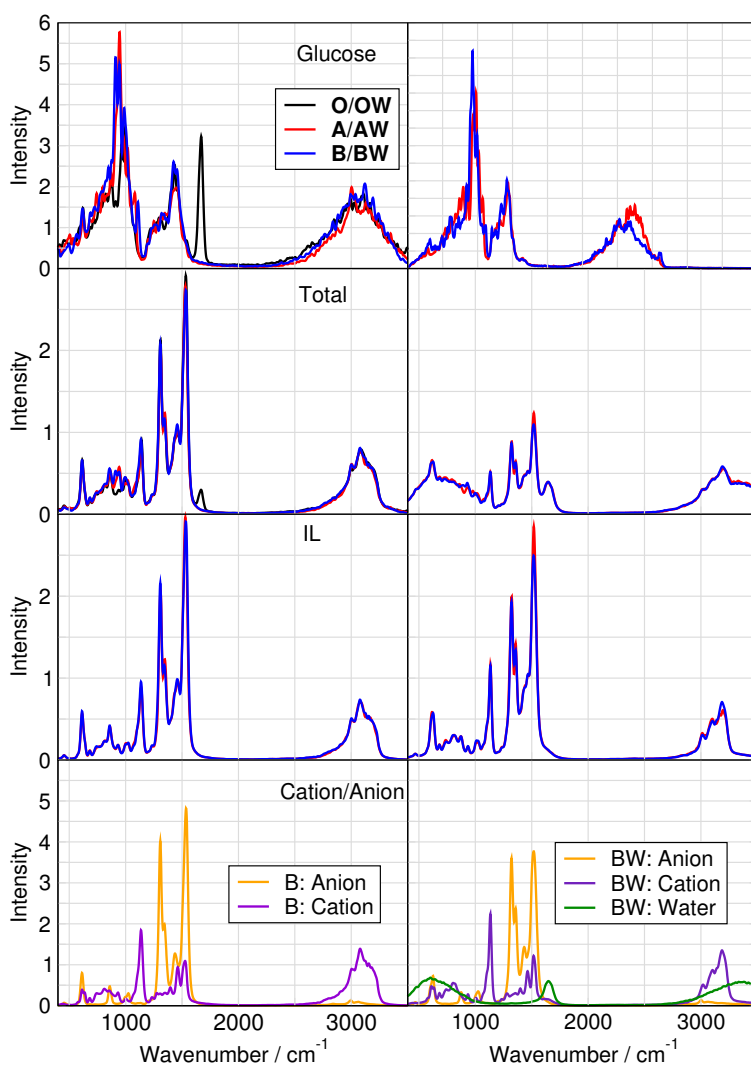


Figure S14: IR spectra of different glucose molecules in $[\text{C}_2\text{C}_1\text{Im}][\text{OAc}]$ with and without water. The left column shows the systems without water, the right column the systems with water. Besides the IR spectra presented for the complete systems, the individual contributions from the glucose and the IL are shown as well.

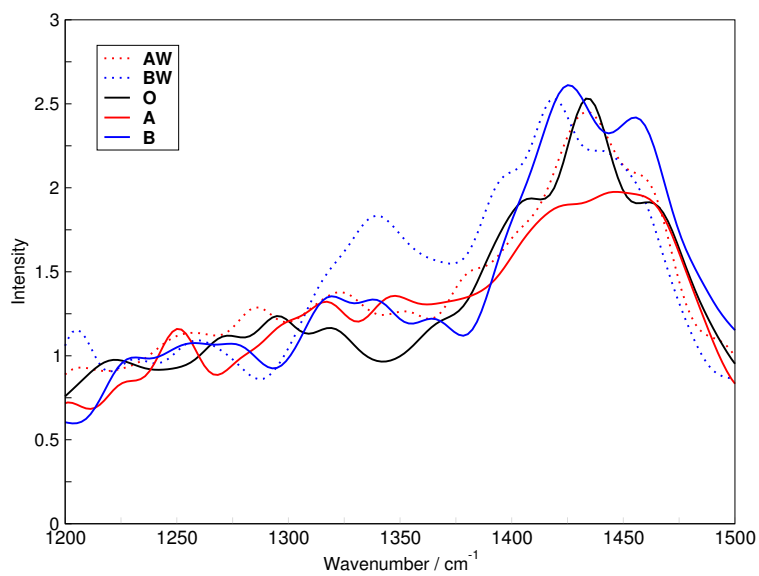


Figure S15: Magnification of the IR spectra of different glucose molecules in [C₂C₁Im][OAc] between 1200 cm⁻¹ and 1500 cm⁻¹ with and without water in order to compare the spectra to experimental data.

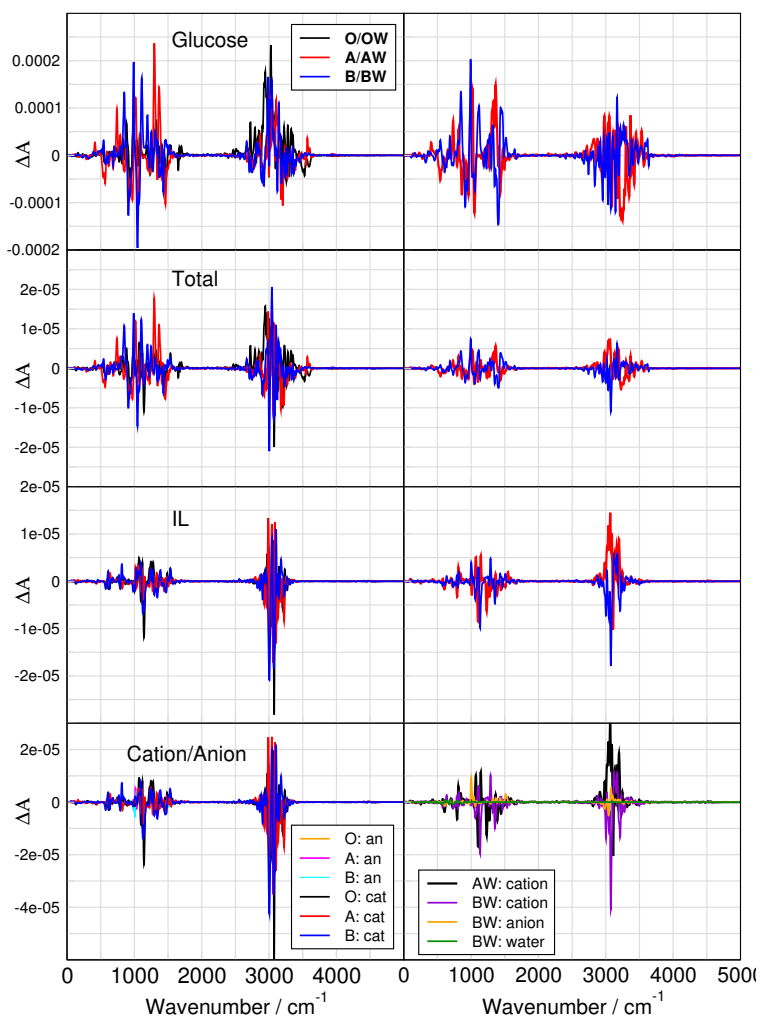


Figure S16: VCD spectra of different glucose molecules in $[C_2C_1Im][OAc]$ with and without water. The left column shows the systems without water, the right column the systems with water. Besides the VCD spectra presented for the complete systems, the individual contributions from the glucose and the IL are shown as well.

3 Acknowledgment

We would like to thank the DFG under the grant project number 406232243.

References

- [1] Martinez, J. M.; Martinez, L. *J. Comp. Chem.* **2003**, *24*, 819–825.
- [2] Martinez, L.; Andrade, R.; Birgin, E. G.; Martinez, J. M. *J. Comp. Chem.* **2009**, *30*, 2157–2164.
- [3] Plimpton, S. *J. Comp. Phys.* **1995**, *117*, 1-19.
- [4] Canongia Lopes, J. N.; Deschamps, J.; Pádua, A. A. H. *J. Phys. Chem. B* **2004**, *108*, 2038-2047.
- [5] Canongia Lopes, J. N.; Pádua, A. A. H. *J. Phys. Chem. B* **2004**, *108*, 16893-16898.
- [6] Canongia Lopes, J. N.; Pádua, A. A. H. *J. Phys. Chem. B* **2006**, *110*, 19586-19592.
- [7] Berendsen, H.; Grigera, J.; Straatsma, T. *J. Phys. Chem.* **1987**, *91*, 6269–6271.
- [8] CP2k developers group under the terms of the GNU General Public License; see <http://www.cp2k.org>.
- [9] VandeVondele, J.; Krack, M.; Mohamed, F.; Parrinello, M.; Chassaing, T.; Hutter, J. *Comput. Phys. Commun.* **2005**, *167*, 103–128.
- [10] VandeVondele, J.; Hutter, J. *J. Chem. Phys.* **2007**, *127*, 114105.
- [11] Goedecker, S.; Teter, M.; Hutter, J. *Phys. Rev. B* **1996**, *54*, 1703–1710.
- [12] Hartwigsen, C.; Goedecker, S.; Hutter, J. *Phys. Rev. B* **1998**, *58*, 3641–3662.
- [13] Krack, M. *Theor. Chem. Acc.* **2005**, *114*, 145–152.
- [14] Grimme, S.; Antony, J.; Ehrlich, S.; Krieg, H. *J. Chem. Phys.* **2010**, *132*, 154104.

- [15] Grimme, S.; Ehrlich, S.; Goerigk, L. *J. Comp. Chem.* **2011**, *32*, 1456–1465.
- [16] Nosé, S. *J. Chem. Phys.* **1984**, *81*, 511–519.
- [17] Hoover, W. G. *Phys. Rev. A* **1985**, *31*, 1695–1697.
- [18] Brehm, M.; Kirchner, B. *J. Chem. Inf. Model.* **2011**, *51*, 2007–2023.
- [19] <http://plasma-gate.weizmann.ac.il/Grace/>.
- [20] <http://www.gnuplot.info/>.
- [21] Brehm, M.; Weber, H.; Thomas, M.; Hollóczki, O.; Kirchner, B. *ChemPhysChem* **2015**, *16*, 3271–3277.
- [22] Green, M. S. *J. Chem. Phys.* **1954**, *22*, 398–413.
- [23] Kubo, R. *J. Phys. Soc. Jpn.* **1957**, *12*, 570–586.
- [24] Wiener, N. *Acta Math.* **1930**, *55*, 117–258.
- [25] Khintchine, A. *Math. Ann.* **1934**, *109*, 604–615.
- [26] Thomas, M.; Brehm, M.; Fligg, R.; Vöhringer, P.; Kirchner, B. *Phys. Chem. Chem. Phys.* **2013**, *15*, 6608–6622.
- [27] Abbate, S.; Longhi, G.; Kwon, K.; Moscovitz, A. *J. Chem. Phys.* **1998**, *108*, 50–62.
- [28] Thomas, M.; Kirchner, B. *J. Phys. Chem. Lett.* **2016**, *7*, 509–513 PMID: 26771403.
- [29] Grimme, S.; Brandenburg, J. G.; Bannwarth, C.; Hansen, A. *J. Chem. Phys.* **2015**, *143*, 054107.
- [30] Zhao, Y.; Truhlar, D. G. *J. Phys. Chem. A* **2005**, *109*, 5656–5667.
- [31] Weigend, F.; Ahlrichs, R. *Phys. Chem. Chem. Phys.* **2005**, *7*, 3297–3305.
- [32] Bannwarth, C.; Ehlert, S.; Grimme, S. *J. Chem. Theory Comput.* **2019**, *15*, 1652–1671.
- [33] Klamt, A. *J. Phys. Chem.* **1995**, *99*, 2224–2235.

- [34] Eckert, F.; Klamt, A. *AIChE J.* **2002**, *48*, 369–385.
- [35] Ahlrichs, R.; Bär, M.; Häser, M.; Horn, H.; Kölmel, C. *Chem. Phys. Lett.* **1989**, *162*, 165-169.
- [36] “TURBOMOLE V7.0 2015, a development of University of Karlsruhe and Forschungszentrum Karlsruhe GmbH, 1989-2007, TURBOMOLE GmbH, since 2007; available from <http://www.turbomole.com>.”, .
- [37] Pensado, A. S.; Brehm, M.; Thar, J.; Seitsonen, A. P.; Kirchner, B. *ChemPhysChem* **2012**, *13*, 1845–1853.
- [38] Firaha, D. S.; Thomas, M.; Hollóczki, O.; Korth, M.; Kirchner, B. *J. Chem. Phys.* **2016**, *145*, 204502.